J|A|C|S ARTICLES

Published on Web 02/16/2009

Photoelectrochemical Study of the Band Structure of Zn_2SnO_4 Prepared by the Hydrothermal Method

Mario A. Alpuche-Aviles and Yiying Wu*

Department of Chemistry, The Ohio State University, Columbus, Ohio 43210

Received August 25, 2008; E-mail: wu@chemistry.ohio-state.edu

Abstract: It is fundamentally interesting to study the photoelectrochemical properties of complex oxides for applications in photovoltaics and photocatalysis. In this paper, we study the band gap (E_g) and energetics of the conduction band (CB) and valence band (VB) for films of zinc stannate (Zn_2SnO_4) nanoparticles (ca. 25 nm) of the inverse-spinel structure prepared by the hydrothermal method. UV−vis spectroscopy, X-ray diffraction (XRD), scanning electron microscopy (SEM), electrochemistry, and photoelectrochemistry were used to study the films. The fundamental E_g for Zn_2SnO_4 is proposed to be 3.6−3.7 eV with a direct-forbidden transition. The position of the CB was approximated from the flat band potential, E_{fb}, measured by the photocurrent onset potential. In aqueous and nonaqueous solutions the E_{fb} of n-Zn_2SnO_4 was found to be more positive than TiO_2 anatase in the electrochemical scale. In aqueous solutions E_{fb} of Zn_2SnO_4 was found to follow a 59 mV/pH slope with E_{fb} extrapolated at pH 0 of 0.08 V vs NHE. In acetonitrile solutions that simulate the electrolyte for dye-sensitized solar cells (DSCs) the E_{fb} of Zn_2SnO_4 was found to be strongly dependent on electrolyte composition and more positive than TiO_2 vs the I^-/I_3^- couple. The reverse trend observed for the open-circuit voltage in certain DSC electrolytes is explained in terms of the higher rates of electron−triiodide recombination of TiO_2 despite the lower position of the Zn_2SnO_4 CB in the vacuum scale.

Introduction

We present a study of the band structure of Zn_2SnO_4 with optical, electrochemical, and photoelectrochemical methods. Zn_2SnO_4 has been proposed as an anode material for dye-sensitized solar cells (DSCs),[1,2] as a transparent conductive oxide (TCO),[3−7] and for Li^+ batteries.[8,9] Its use has also been demonstrated for the photocatalytic decomposition of benzene[10] and methylene blue.[11] From a fundamental point of view, it is interesting to study Zn_2SnO_4 as a model ternary oxide to understand how the optical and electronic properties are controlled by composition and structure.

The growing interest in complex oxides comes as the properties of binary oxides, while well established in several areas, seem to limit the performance of new applications. This is particularly interesting in energy applications where there is a demand for specially designed semiconductors to better match the properties of emerging materials. For example, for CdTe/CdS solar cells, the incident light to power conversion efficiency (1 sun, AM 1.5), η, was improved from 13.5% (SnO_2 as TCO) to 15.8% when $Zn_2SnO_4/SnCd_2O_4$ was the TCO in the device.[12]

Recently, DSCs have attracted attention as an alternative to solid-state devices due to their low fabrication cost and relatively high efficiency.[13] The motivation for replacing the widely used TiO_2 comes from the limitations that have become apparent in the recent literature: The use of TiO_2 anatase with $E_g = 3.2$ eV presents the problem of dye photobleaching by the UV region of the solar spectrum. There has been a lot of interest in the development of new sensitizers for efficient light harvest, which

(1) Tan, B.; Toman, E.; Li, Y.; Wu, Y. *J. Am. Chem. Soc.* **2007**, *129*, 4162.
(2) Lana-Villarreal, T.; Boschloo, G.; Hagfeldt, A. *J. Phys. Chem. C* **2007**, *111*, 5549.
(3) Enoki, H.; Nakayama, T.; Echigoya, J. *Phys. Status Solidi A* **1992**, *129*, 181.
(4) Satoh, K.; Kakehi, Y.; Okamoto, A.; Murakami, S.; Uratani, F.; Yotsuya, T. *Jpn. J. Appl. Phys., Part 2* **2005**, *44*, L34.
(5) Coutts, T. J.; Young, D. L.; Li, X.; Mulligan, W. P.; Wu, X. *J. Vac. Sci. Technol., A* **2000**, *18*, 2646.
(6) Young, D. L.; Moutinho, H.; Yan, Y.; Coutts, T. J. *J. Appl. Phys.* **2002**, *92*, 310.
(7) Segev, D.; Wei, S.-H. *Phys. Rev. B: Condens. Matter Mater. Phys.* **2005**, *71*, 125129/1.
(8) Rong, A.; Gao, X. P.; Li, G. R.; Yan, T. Y.; Zhu, H. Y.; Qu, J. Q.; Song, D. Y. *J. Phys. Chem. B* **2006**, *110*, 14754.
(9) Belliard, F.; Connor, P. A.; Irvine, J. T. S. *Solid State Ionics* **2000**, *135*, 163. Connor, P. A.; Irvine, J. T. S. *J. Power Sources* **2001**, *97−98*, 223.
(10) Cun, W.; Wang, X. M.; Zhao, J. C.; Mai, B. X.; Sheng, G. Y.; Peng, P. A.; Fu, J. M. *J. Mater. Sci.* **2002**, *37*, 2989.
(11) Zeng, J.; Xin, M.; Li, K.; Wang, H.; Yan, H.; Zhang, W. *J. Phys. Chem. C* **2008**, *112*, 4159.
(12) Wu, X.; Asher, S.; Levi, D. H.; King, D. E.; Yan, Y.; Gessert, T. A.; Sheldon, P. *J. Appl. Phys.* **2001**, *89*, 4564.
(13) (a) Oregan, B.; Gratzel, M. *Nature* **1991**, *353*, 737. (b) Martin, A.; Green, K. E.; Hishikawa, Y.; Warta, W. *Prog. Photovolt.: Res. Appl.* **2008**, *16*, 435. (c) Chiba, Y.; Islam, A.; Kakutani, K.; Komiya, R.; Koide, N. H. High efficiency dye sensitized solar cells. *Technical Digest, 15th International Photovoltaic Science and Engineering Conference*; Shanghai Science and Technology Press: Shanghai, 2005. (d) Chiba, Y.; Islam, A.; Watanabe, Y.; Komiya, R.; Koide, N.; Han, L. *Jpn. J. Appl. Phys., Part 2* **2006**, *45*, L638. (e) Gratzel, M. *J. Photochem. Photobiol., A* **2004**, *164*, 3. (f) Mor, G. K.; Shankar, K.; Paulose, M.; Varghese, O. K.; Grimes, C. A. *Nano Lett.* **2006**, *6*, 215. (g) Nazeeruddin, M. K.; Pechy, P.; Renouard, T.; Zakeeruddin, S. M.; Humphry-Baker, R.; Comte, P.; Liska, P.; Cevey, L.; Costa, E.; Shklover, V.; Spiccia, L.; Deacon, G. B.; Bignozzi, C. A.; Graetzel, M. *J. Am. Chem. Soc.* **2001**, *123*, 1613.

10.1021/ja806719x CCC: $40.75

Table 1. Summary of E_g values of Zn_2SnO_4

sample preparation and comments	Zn/Sn[a]	method	E_g (eV)	transition	ref
RF magnetron sputtering (500 °C Ar + O) and heat treated at 750 °C, 1 h in air; I-spinel;[b] E_g increased with annealing temperature	2.0	film absorbance	4.1	d.a.[c]	4
RF magnetron sputtering from sintered ZnO and Sn_2O; *e*-diffraction pattern consistent with I-spinel; from transmittance cutoff at $\lambda < 320$ nm	n/a	film absorbance	3.9	n/a	3
RF sputtering (680 °C in Ar), amorphous	n/a[d]	n/a	~3.6	n/a	5
RF sputtering; I-spinel; E_g	1.8	extrapolated	3.35 ± 0.09	d.a.	6
extrapolated from optical measurements showing normal Burstein−Moss effects: higher band gap with higher dopant concentration		max optical	3.85	d.a.	
hydrothermal; I-spinel	n/a			n/a	23
2−4 nm in diameter and around 20 nm in length		diffuse reflectance	3.87		
500 nm particles			3.67		
LDA;[e] calculation for stoichiometric Zn_2SnO_4; normal and inverse-Moss-Burstein shifts predicted	2.00				7
normal-spinel		calculation	0.5	d.f.[f]	
I-spinel		calculation	1.7	d.f.	
		error est.	+1.4		
hydrothermal, I-spinel, NPs film	2.07 ± 0.02				this work
as prepared		optical	3.71 ± 0.04	d.f.	
heat treated		optical	3.25 ± 0.03	d.f.	
heat treated		PEc[g]	3.86 ± 0.08		
proposed			3.6−3.7	d.f.	

[a] Molar ratio as reported, when available. [b] I-spinel: inverse spinel. [c] d.a.: direct allowed, eq 3. [d] n/a: not available. [e] LDA: local density approximation. [f] d.f.: direct forbidden, eq 4. [g] PEc: photoelectrochemistry.

also requires appropriate support with optimum energy alignment. Thus, we are exploring new materials to optimize energy matching and decrease the rate of recombination between photogenerated electrons, *e*, and triiodide. Several oxides, and oxide combinations have been reported (for a review see ref 14), although so far the highest certified η is for DSCs based on TiO_2 nanoparticles (NPs). To the best of our knowledge, $SrTiO_3$ ($\eta = 1.8\%$)[15] and Zn_2SnO_4 are the only two ternary oxides reported for DSCs support.

There are a couple of reports for Zn_2SnO_4 as the DSC photoanode: Lana-Villareal et al.[2] and Tan et al. (our group).[1] Both reports agree in that Zn_2SnO_4 is a promising material for DSCs: our group found the promising $\eta = 3.8\%$,[1] and Villareal et al. found similar effective *e*-diffusion coefficients for TiO_2 and Zn_2SnO_4 while the *e*-lifetime was larger for Zn_2SnO_4 than for TiO_2. However, these reports are contradictory in that the open circuit voltage of the DSCs, V_{oc} presents different trends with respect to TiO_2. These differences have been ascribed to the relative positions of the conduction band of Zn_2SnO_4 with one report claiming a lower conduction band edge,[1] E_{cb}, and the other a higher E_{cb} of Zn_2SnO_4 with respect to TiO_2 in the vacuum scale.[2]

Studies of the band structure of Zn_2SnO_4 are scarce.[3−7] While studies of binary oxides (TiO_2, SnO_2, etc.) have been carried out extensively, there are still relatively few studies of complex oxides. For Zn_2SnO_4 most studies are in the context of the TCO, i.e., calculating[7] and measuring the optical[3−6] and transport properties as a function of doping concentration, especially under different preparation and annealing conditions. However, these properties are not well established; for example, the reported band gap, E_g, varies from 3.35 to 4.1 eV (see Table 1).

In this paper, we study the band-gap and energy positions of the conduction band (CB) and valence band (VB) of Zn_2SnO_4 in aqueous and nonaqueous solution. The position of the CB is approximated by the flat band potential, E_{fb}, which is a good approximation of the Fermi level, E_F.

The relative positions of E_{fb} for Zn_2SnO_4 and TiO_2 in aqueous and nonaqueous solutions are presented, and overall, those of Zn_2SnO_4 were found to be more positive in the electrochemical scale (more negative in the vacuum scale). The E_{fb} measurements in MeCN solutions that simulate the electrolyte for the DSCs explain the contradictory reports of V_{oc} in terms of the relative rates of electron−triiodide recombination for the different materials.[1,2]

Experimental Methods

Chemicals and Materials. All chemicals were used as received. $ZnCl_2$ (98%), $SnCl_4 \cdot 5H_2O$ (98%), titanium tetraisopropoxide (98%), LiI (99.9%), I_2 (99.99%), tetra-*n*-butylammonium iodide (99%), 4-*tert*-butylpiridine (99%), and Triton X were purchased from Sigma-Aldrich (St. Louis, MO), tetra-*n*-butylammonium perchlorate (98%) and polyethylene glycol (MW = 20 000) from Alfa Aesar (Ward Hill, MA), *tert*-butylamine (99%) from Across Organics (Geel, Belgium), HCl and HNO_3 (ACS plus) from Fisher Scientific (Pittsburgh, PA), and 1,2-dimethyl-3-propylimidazolium iodide (DMI) was a gift from Shikoku Chemicals Co. (Japan). Aqueous solutions were prepared with water from a Barnstead E-Pure system (18 MΩ cm). Nonaqueous solutions were prepared in acetonitrile (MeCN, Puriss Anhydrous) from Sigma-Aldrich stored in an Ar glove box (Vacuum Atmospheres Co, Hawthrone, CA) where solutions were prepared and stored.

Metal Oxides Preparation. Nanoparticles of Zn_2SnO_4 and TiO_2 were prepared by the hydrothermal method according to previously reported procedures.[1,16,17] Briefly, Zn_2SnO_4 was prepared according to our previous report[1] from stoichiometric amounts of $ZnCl_2$ and $SnCl_4 \cdot 5H_2O$ with *tert*-butylamine as the coordinating agent at 170 °C, 12 h. The precipitate was purified by dispersion and centrifugation in water, water−ethanol mixtures, and ultimately ethanol. TiO_2 was prepared following a modified[16] procedure of Zaban et al.:[17] a titanium isopropoxide solution in 2-propanol was dissolved

(14) Arakawa, H.; Hara, K. Current status of dye-sensitized solar cells. In *Semiconductor Photochemistry and Photophysics*; Ramamurthy, V., Schanze, K. S., Eds.; Marcel Dekker: New York, 2003; Vol. 10, p 123.
(15) Burnside, S.; Moser, J. E.; Brooks, K.; Gratzel, M.; Cahen, D. *J. Phys. Chem. B* **1999**, *103*, 9328.
(16) Tan, B.; Wu, Y. *J. Phys. Chem. B* **2006**, *110*, 15932.
(17) Zaban, A.; Ferrere, S.; Sprague, J.; Gregg, B. A. *J. Phys. Chem. B* **1997**, *101*, 55.

dropwise in acetic acid solutions. This solution was heated at 240 °C for 12 h to yield an anatase suspension used without further purification. Films were prepared by the doctor blade method from Zn_2SnO_4 dispersions with Triton X and acetyl acetone or from a TiO_2 paste. The TiO_2 paste was prepared by adding polyethylene glycol (FW = 20 000) by 10% w/w relative to TiO_2 and evaporated to a spreadable paste for the right film thickness. The films were allowed to dry overnight and then heat treated at 500 °C for 30 min (3 °C heating and max cooling ramp). Films were prepared on F-doped SnO_2 (FTO Tec 8, Pilkington North America, Toledo, OH) for electrochemical measurements, on glass slides for XRD measurements, and on silica slides for Zn_2SnO_4 optical transmittance studies. Film thickness (typically 10−20 μm) was measured with a profilometer (Dektak 3).

Metal Oxide Characterization. The NPs were characterized by X-ray powder diffraction (XRD, Cu Kα, Geirgerflex, Rigaku Co, Japan) and the films by scanning electron microscopy (SEM, Sirion, FEI Co., Hillsboro, OR). The Zn/Sn ratio in Zn_2SnO_4 was determined by ICP-MS (Elan 6000, Perkin-Elmer, Waltham, MA) at the Microscopic and Chemical Analysis Research Center at OSU; Zn_2SnO_4 samples were digested in 3:1 v/v HCl:HNO_3 (conc) and ultimately diluted to ca. 400 ppb in 2% HNO_3 v/v. UV−vis spectra were obtained with a Lambda 950 spectrophotometer (Perkin-Elmer) with a 60 mm integrating sphere. Spectra were collected with 1 nm resolution in the transmittance and total reflectance modes. The film absorbance spectra were calculated from the absorbance of the film by correcting the transmittance for the total reflectance.

Electrochemical and Photoelectrochemical Measurements. A Reference 600 (Gamry Instruments, Warminster, PA) or a CV50W (Bioanalytical Systems, West Lafayette, IN) potentiostat was used for our measurements. A 200 W Hg lamp (Oriel, Stratford, CT) with a water IR filter (Oriel) was used to illuminate the samples with a chopping frequency of 0.05 Hz and a scan rate $\nu = 1$ mV/s in all photoelectrochemical experiments. A Cornerstone 130 monochromator (Oriel) with a 20 nm resolution slit and a Si photodiode detector (OPM-1830C, Newport Co., Irvine, CA) were used to study the dependence on wavelength, λ.

The flat band potential, E_{fb}, was measured by the photocurrent onset method described elsewhere.[18,19] Experiments in aqueous solution were done in 1 M KCl, 1 M acetate (AcO^-) adjusted to the right pH with HCl, acetic acid, or KOH. The cell was made out of Teflon with a flat silica window. The reference electrode was a Ag/AgCl (KCl saturated, Gamry) with a Vycor tip. The counter electrode was a Pt mesh and was kept in a compartment separated with a porous glass frit. All solutions were purged with Ar for at least 30 min before experiments. Samples were kept in air and illuminated from the front side.

For experiments in MeCN, the films were allowed to cool to 120 °C after heat treatment and transferred to a glovebox with an Ar atmosphere for storage. FTO blanks were heat treated as described above for the films and were immediately transferred to the Ar glovebox. All samples were exposed to the atmosphere only long enough to mount them in a specially designed Teflon cell; the setup was immediately transferred to the glovebox, where the cell was loaded with the solutions and closed. Cyclic voltammetry (CV) was conducted with the closed cell in the dry box, and photoelectrochemical experiments were done with the sealed cell transferred outside the box and under back-side illumination.

The reference electrode for experiments in nonaqueous solutions was a Pt wire immersed in a 10 mM I^-/I_3^- solution in MeCN kept in a borosilicate glass capillary with a soft glass-cracked junction (homemade). The solution was prepared from 20 mM tetrabutyl ammonium iodide, 10 mM iodine, and 0.2 M tetrabutylammonium perchlorate (TBAP) used as supporting electrolyte. The reference was always used with a double junction: a glass tube with a glass-cracked junction filled with 0.2 M TBAP; the counter electrode was a Pt coil.

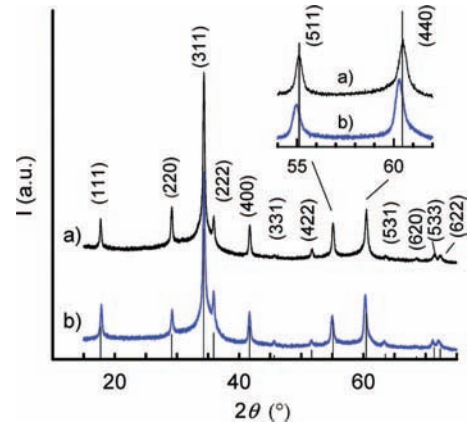

Figure 1. X-ray (Cu Kα) diffraction of a film of Zn_2SnO_4 NPs showing inverse spinel (a) as prepared and (b) after heating at 500 °C (30 min) with a 3 °C/min heating and max cooling ramp in stagnant air. PDF #24-1470 pattern is shown for comparison (vertical lines). The insert shows the shift in peak positions for planes (511) and (400) consistent with an increase (0.3%) in the lattice constant, a, after heating. From PDF: (511) 2θ = 55.114°, (440) 2θ = 60.440°, a = 8.657 Å. Particle size calculated from the as-prepared NPs is 25 ± 3 nm

Results

Material Characterization. Both TiO_2 and Zn_2SnO_4 were characterized by XRD and SEM. The XRD pattern for Zn_2SnO_4 film of NPs used as prepared is presented in Figure 1a. This pattern matches the Powder Diffraction File (PDF #24-1470) of The International Center for Diffraction Data.[20] Zn_2SnO_4 presents a spinel structure; the XRD difference for the normal and inverse-spinel forms has been described in detail elsewhere.[21] Briefly, the "degree of inversion" is defined as x in eq 1a[21]

$$(Sn_{1-x}Zn_x)[Sn_xZn_{2-x}]O_4 \quad (1a)$$

where the part in parentheses represents the tetrahedral sites and in square brackets the octahedral sites. If $x = 0$ the structures is normal spinel, i.e., only Sn in tetrahedral sites. For our material we estimate a value of $x = 0.9$ using the method of Young et al., although this method has limitations in resolving small differences in degrees of inversion.[21] Thus, we assume a fully inverted spinel structure where all the tetrahedral sites are occupied by Zn as in eq 1b

$$(Zn)[Sn\ Zn]O_4 \quad (1b)$$

The inverse-spinel structure in eq 1b is the one obtained by the hydrothermal method used in this work and other reports.[1,2,8,22,23] This has been calculated to be the most thermodynamically stable configuration[7,24] and is expected to form under hydrothermal conditions.

The XRD pattern shows changes when the films were heat treated at 500 °C for 30 min like the films used in our

(18) Butler, M. A. *J. Appl. Phys.* **1977**, *48*, 1914.
(19) Finklea, H. O. Semiconductor Electrode: Concepts and Terminology. In *Semiconductor Electrodes*, 1st ed.; Finklea, H., O., Ed.; Elsevier: Amsterdam, 1988; Vol. 55, p 1.
(20) Swanson, H. E.; McMurdie, H. F.; Morris, M. C.; Evans, E. H.; Paretzkin, B. *Natl. Bur. Stand. (U.S.) Monogr.* **1972**, *25*, 62.
(21) Young, D. L.; Williamson, D. L.; Coutts, T. J. *J. Appl. Phys.* **2002**, *91*, 1464.
(22) Fang, J.; Huang, A.; Zhu, P.; Xu, N.; Xie, J.; Chi, J.; Feng, S.; Xu, R.; Wu, M. *Mater. Res. Bull.* **2001**, *36*, 1391.
(23) Zhu, H.; Yang, D.; Yu, G.; Zhang, H.; Jin, D.; Yao, K. *J. Phys. Chem. B* **2006**, *110*, 7631.

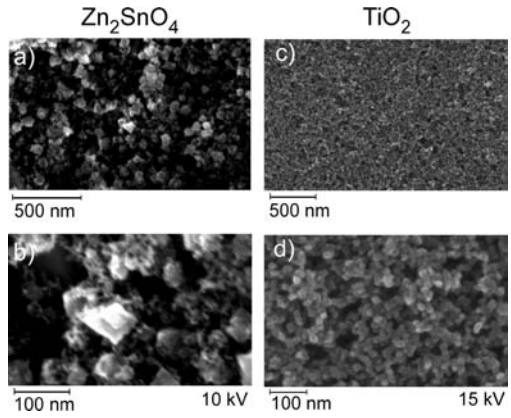

Figure 2. Scanning electron micrographs annealed films of nanoparticles of Zn_2SnO_4 (a and b) and TiO_2 anatase (c and d) used in this study.

electrochemical studies (Figure 1b). The higher index planes shifted toward lower 2θ values, i.e., higher d spacing, while the lower index planes remained constant with no change in the degree of inversion. This shift is consistent with a change in the lattice constant that we calculated to be 0.3%.

The average particle size calculated from the XRD for the as-prepared Zn_2SnO_4 particles from the (111), (220), (311), (400), (511), and (440) planes is 25 ± 3 nm (error from the sample standard deviation) and within experimental error of the calculated size after heat treatment; we found no evidence of stress-induced artifacts. This is consistent with the measurements by transmission electron microscopy (TEM) of previous reports: 10−60 nm under these conditions[1] and 27 nm with different conditions.[2] The TiO_2 prepared and used in this work shows XRD patterns consistent with anatase (not shown) and a particle size of 18 nm, consistent with TEM in our previous report.[16] The films used in this work are compared in Figure 2: while the average particle sizes are similar, TiO_2 has a much narrower particle size distribution than Zn_2SnO_4.

The actual Zn to Sn molar ratio was determined by ICP-MS after dissolving samples from three separate batches with the following molar ratios: sample A, 2.11 ± 0.04; B, 2.03 ± 0.03; C, 2.09 ± 0.02; average, 2.07 ± 0.02. It is clear from these measurements that the hydrothermal method in our conditions has a tendency to produce materials with a small excess of Zn despite the initial stoichiometric amount used.

Band-Gap (E_g) Measurements. Optical and photoelectrochemical measurements were performed to determine the E_g of our material. The absorbance of NP films as prepared (4 μm) and after heat treatment (2 μm) corrected for the total reflection are shown in Figure 3a. Note that the heat-treated sample shows a shift of the absorbance cutoff to higher wavelengths, λ (in nm), which indicates a decrease in the optical E_g with heat treatment. Also, from the absorbance of the silica support (dotted line) the absorbance feature at ca. 230 nm is due to the support.

The absorption coefficient α (in cm^{-1}) is calculated according to eq 2[25]

$$\alpha = \frac{1}{d} \ln \frac{I_o}{I} \tag{2}$$

where d is the film thickness (in cm) and I_o and I are the incident and transmitted light intensities, respectively. We note that in our experiments the films are made of NPs, and thus, the apparent α that we measure, α_{NP}, shown in Figure 3b are not expected to match the values for continuous films or a single crystal, although α_{NP} measurements are relevant for applications of these films, e.g.,

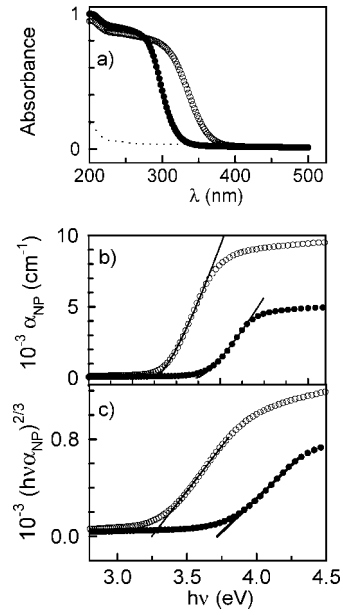

Figure 3. Optical band-gap (E_g) measurements of Zn_2SnO_4 films of NPs (●) as prepared and after (○) heat treatment and (---) silica support. (a) Film absorbance showing red shift after heat treatment. (b) Apparent absorption coefficient (α_{NP}) of NPs films as a function of photon energy ($h\nu$); lines show the theory of direct-forbidden transitions. (c) Calculation of E_g for direct-forbidden transition (see eq 4) from the x intercept of the (●) as-prepared NPs film (E_g = 3.71 ± 0.04 eV) and the (○) heat-treated film (E_g = 3.25 ± 0.03 eV).

DSCs. We are unaware of any report using Zn_2SnO_4 single crystal, but for continuous films our values of $\alpha_{NP} \leq 10^4$ are in good agreement with the reported[6] $\alpha \leq 2.5 \times 10^4$ for doped films with different stoichiometry (see Table 1) and also within the expected values from theoretical calculations[7] with $\alpha < 20 \times 10^4$. Thus, although the actual values of α_{NP} from eq 2 may contain errors due to the film morphology (see Figure 2a and 2b) the dependence on wavelength can be used to study the band to band transitions.

The dependence of α on photon energy ($h\nu$) is characteristic of the transition type: if the transition is "direct allowed" α will follow eq 3[26,27]

$$\alpha = B_{da} \frac{(h\nu - E_g)^{1/2}}{h\nu} \tag{3}$$

and if it is "direct forbidden" it will follow eq 4[26,27]

$$\alpha = B_{df} \frac{(h\nu - E_g)^{3/2}}{h\nu} \tag{4}$$

where α is in cm^{-1}, B_{da} and B_{df} are characteristic constants for each material and transition, $h\nu$ is the incident photon energy (in eV), and E_g is the material band gap in eV.

Our data best fits the direct-forbidden transitions, i.e., eq 4 for films of NPs as prepared and heat treated; these lines are shown in Figure 3b and 3c. The value of $B_{df} = 3.7 \times 10^4$ and 5.7×10^4 cm^{-1} obtained for the as-prepared and heat-treated samples agree well with the values of 1.3×10^4 (ref 26) and 4.5×10^4 cm^{-1} (ref 27) suggested for this transition. In Figure

(24) Wei, S.-H.; Zhang, S. B. *Phys. Rev. B* **2001**, *63*, 045112.
(25) Memming, R. *Semiconductor Electrochemistry*; Wiley-VCH: Weinheim, 2001.
(26) Pankove, J. I. *Optical Processes in Semiconductors*; Prentice-Hall: Eglewood Cliffs, NJ, 1971.
(27) Smith, R. A. *Semiconductors*, 2nd ed.; Cambridge University Press: Cambridge, 1978.

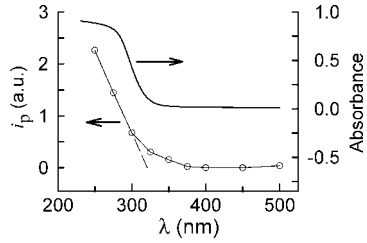

Figure 4. Photocurrent (i_{ph}) action spectrum of Zn_2SnO_4 after heat treatment (○). The x intercept of the rising part of the i_p curve (321 nm) yields E_g = 3.86 eV (extrapolation error ± 0.08 eV). E = 0.2 V vs NHE, 1 M KCl, 1 M AcO^-, pH 4.8. For comparison, the optical absorbance of a film before heat treatment is also shown (—).

3c the data has been converted to $(h\nu\alpha_{NP})^{2/3}$ vs $h\nu$ to calculate the E_g from the x intercept, yielding $E_g = 3.71 \pm 0.04$ eV for the as-prepared NPs and 3.25 ± 0.03 eV after heat treatment. As discussed below, this difference in E_g with heat treatment is believed to be the result of excess Zn incorporating into the Zn_2SnO_4 matrix.

The band gap was also measured by photoelectrochemistry. Figure 4 shows the photoelectrochemical E_g measurement for a heat-treated film from the photocurrent (i_{ph}) action spectrum: i_{ph} as a function of the normalized power at different wavelengths. For comparison, the optical E_g measurement for a film before heat treatment (same as Figure 3a) is also shown. The substrate was kept at a potential of E = 0.2 V vs NHE in 1 M KCl, 1 M AcO^-, pH 4.8. Under these conditions, the i_{ph} measured corresponds to e promoted from the VB to the CB by photons absorbed by the semiconductor. The photogenerated holes (h^+) oxidize the AcO^- present in high concentration to prevent h^+ from damaging the Zn_2SnO_4 substrate. Thus, the rising part of i_{ph} can be used to extrapolate a cutoff λ = 321 nm that yields $E_g = 3.86 \pm 0.08$ eV. The E_g for this heat-treated sample is within experimental error of the as-prepared sample with optical measurements (3.71 ± 0.04 eV). Note that the errors shown come from the uncertainty of the extrapolation and do not take into account the actual resolution of the measurement. To obtain the i_{ph} action spectra our experimental setup limits us to a slit of a 20 nm resolution to maximize throughput and obtain a measurable i_{ph}; thus, it is not possible to obtain as many significant points as with the optical measurements (Figure 3) or use the i_{ph} dependence on λ to study the transition type. Nevertheless, the i_{ph} shows a clear trend with average λ and is used to obtain E_g. As discussed below, under these conditions the E_g measured should correspond to the fundamental transition. Figure 4 also shows the close correlation between the E_g measured by photoelectrochemistry and the optical E_g before heat treatment, and discussed below, this indicates the electronic E_g of the material to be 3.6−3.7 eV

***E_{fb}* Measurements.** We measured E_{fb} using the photocurrent onset potential for films prepared after heat treatment. Although the average size of individual Zn_2SnO_4 nanoparticle is 25 nm, there are particles as large as 100 nm (Figure 2). Moreover, heat treatment causes the nanoparticles to agglomerate. Thus, we believe that the particles can support the space-charge layer and the concept of flat-band potential holds here. The bands are not flat and they bend updwards or downward depending on the experimental conditions.

Figure 5 shows measurements of E_{fb} in aqueous solution. Figure 5a shows the photocurrent of Zn_2SnO_4 in 1 M KCl, 1 M AcO^-, pH 4.8 with the light from a 200 W Hg lamp being chopped. The photocurrent becomes apparent at ca. −0.2 V vs

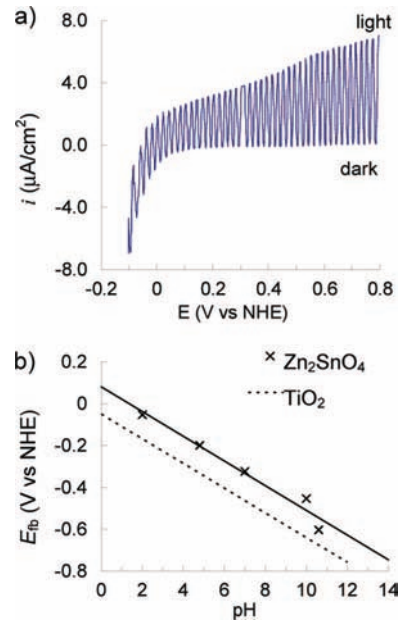

Figure 5. Flat band potential (E_{fb}) measurements in aqueous electrolyte. (a) Photocurrent as a function of potential at pH 4.8 (1 M KCl and 1 M AcO^-) ν = 1 mV/s, 200 W Hg lamp, 0.05 Hz chopping frequency. (b) E_{fb} for NP films of (×) Zn_2SnO_4. The lines show pH dependence for (—) Zn_2SnO_4 with a 59 mV/pH slope and E_{fb}(pH = 0) = 0.08 V vs NHE and (- - -) TiO_2 NPs suspension, ref 30.

NHE as the current becomes more positive, i.e., anodic, under illumination and increases in magnitude in the positive direction. At potentials more negative than −0.2 V negative currents in the dark result from cathodic faradaic processes. This is consistent with Zn_2SnO_4 moving from a degenerate-type behavior into the forbidden E_g region as the Fermi level of the electrode is scanned positive in the electrochemical scale (negative in the solid-state vacuum scale) and with the onset of the photocurrent corresponding to the E_{fb}. The increase of the photocurrent slope at around 0.4 V vs NHE is believed to be due to the photooxidation of the O^{2-} in the oxide material to O_2.[28]

We note that as the background "dark" current increases in the cathodic direction there is also a weak cathodic photocurrent for the n-Zn_2SnO_4. This behavior has been reported before, although to the best of our knowledge it is not completely clear what makes the background current depend on light intensity at potentials beyond the E_{fb} and into the degenerate-metallic region of the semiconductor. Finklea[19] pointed out that for an n-type material a photocathodic current is observed at potentials more negative of the E_{fb} this current is small because at this degenerated condition photoexcitation does not significantly increase the surface carrier concentration. Bard and Kohl[29] reported under intense illumination that the electrode surface can heat and cause convection of the redox species while increasing the conductivity of the semiconductor. Both effects

(28) Scaife, D. E. *Sol. Energy* **1980**, *25*, 41.
(29) Bard, A. J.; Kohl, P. A. The Semiconductor-Nonaqueous Solution Interface—Characterization and Applications. In *Semiconductor Liquid-Junction Solar Cells: Proceedings of a Conference on the Electrochemistry and Physics of Semiconductor Liquid Interfaces under Illumination*; Airlie, Virginia, May 3–5, 1977; Heller, A.; Ed.; Electrochemical Society: Princeton, NJ, 1977; Vol. 77–3, pp 222–230.
(30) Ward, M. D.; White, J. R.; Bard, A. J. *J. Am. Chem. Soc.* **1983**, *105*, 27.

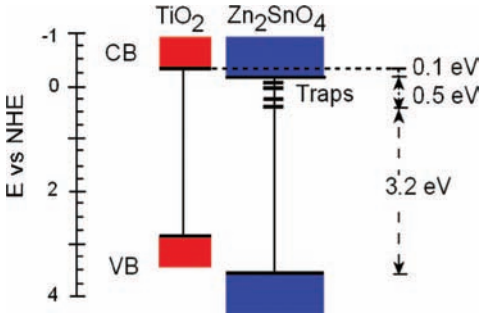

Figure 6. Comparative energy diagram of TiO_2 ($E_g = 3.2$ eV) and Zn_2SnO_4 ($E_g = 3.7$ eV) in aqueous solution at pH 4.8; for simplicity, the surface states in TiO_2 near the CB are not shown. CB drawn assuming $E_F = E_{fb} \approx E_{cb}$

increase the cathodic current under illumination of an n-type semiconductor. We have not attempted to study this weak photocurrent, but we note that we observed this effect for both aqueous (Figure 5a) and nonaqueous solutions (see below).

Figure 5b shows the results of the E_{fb} as a function of pH. The solid line corresponds to a 59 mV/pH change with an extrapolated E_{fb} (pH 0) = 0.08 V. The dotted line in the Figure 5b corresponds to measurements of TiO_2 anatase particles of 200 nm diameter in suspension with E_{fb} (pH 0) = −0.05 V;[30] for TiO_2 films of our 18 nm NPs we found our data to scatter around the line in Figure 5b,[30] which is only 0.09 V positive of the one reported for 20 nm particles in suspension.[31] The E_{fb} of Zn_2SnO_4 is consistently more positive than that of TiO_2 by ca. 0.1 V. The diagram in Figure 6 is constructed by combining the information of E_{fb} and E_g for both materials and includes the traps that account for our optical and photoelectrochemical measurements of E_g and E_{fb}. This diagram was drawn assuming $E_{fb} = E_{cb}$, although E_{fb} is a good approximation of E_F. The difference between E_{cb} and E_{fb} is set by the free carrier density, N_{sc}. It was not possible to measure N_{sc} of our films using the Hall mobility since the high concentration of grain boundaries causes electron transport through the NP film to be trap-limited. We are currently pursuing measurements of N_{sc} using electrochemical and capacitance measurements that will be presented elsewhere. Our results indicate that for Zn_2SnO_4 the minimum N_{sc} is 1.2×10^{17} cm^{-3}, which will make the difference between E_c and $E_F \approx 140$ mV maximum. The TiO_2 NPs will also have a difference in E_c and E_{fb} (or E_F) that will depend on their N_{SC}, which has the same measuring problems as those of Zn_2SnO_4. Thus, to be fair, we neglect these differences and approximate E_c with E_{fb} for both materials in the energy diagram (Figure 6) and note that this trend in E_c for TiO_2 and Zn_2SnO_4 is consistent with previous DSCs results[1] and measurements in nonaqueous electrolyte.

In nonaqueous solutions using MeCN as the solvent the E_{fb} measured under different conditions is shown in Table 2. Our data also shows that the trend of E_{fb} for Zn_2SnO_4 is more positive than that of TiO_2. Note that our data is referred to the 10 mM I^-/I_3^- reference electrode that we prepared for this work; to a first approximation, from the Nernst equation the estimated potential is ca. 0.65 V vs NHE. Thus, our data for TiO_2 of −0.7 to −0.8 V vs I^-/I_3^- (10 mM) would correspond to −0.05 to −0.15 V vs NHE, which is not in accordance with the generally accepted value of −0.5 V vs NHE.[14,32] We did not attempt to accurately calibrate our reference since our goal is to compare E_{fb} measurements of Zn_2SnO_4 with TiO_2 under the exact same conditions.

Table 2. E_{fb} Measurements for TiO_2 Anatase and Zn_2SnO_4 in MeCN[a] Solutions

	E_{fb} (V vs I^-/I_3^- 10 mM)	
conditions	TiO_2	Zn_2SnO_4
0.2 M TBAP[b]	−0.77	−0.26
DSCE,[c] No TBP[d]	−0.67	−0.51
DSCE + 0.5 M TBP	−0.85	−0.69
0.7 M LiI, 0.05 M I_2 (No TBP)	−0.80	−0.60

[a] Solvent: MeCN Puriss Anhydrous, as received. [b] TBAP: tetra-*n*-butylammonium perchlorate. [c] DSCE: 0.02 M I_2, 0.04 M LiI, 0.5 M, 0.5 M 1,2-dimethyl-3-propylimidazolium iodide. [d] TBP: 4-*tert*-butyl pyridine.

The E_{fb} of TiO_2 is somewhat constant despite the different electrolyte compositions, consistent with the reported trend of TiO_2 of E_{fb} in high concentrations (>0.01 M) of Li^+,[33] measured by "optical electrochemistry".[34] However, the differences in our reported values and those from the measurements in optical electrochemistry measurements[33] could be due to several factors. (1) There are many discrepancies in E_{fb} measurements for TiO_2 in MeCN: measurements with the Mott−Schottky method before (ca. −2 V) and after illumination (ca. 0 V vs NHE) of E_{fb} of TiO_2 for single crystals vary in +2 V,[35,36] and there is a difference between the E_{fb} from the photocurrent (−0.6 V) and Mott−Schottky methods (<−1 V);[37] this could be due to the photo-oxidation of the electrolyte or traces of water[35] that modified the liquid/TiO_2 interface or relaxation phenomena caused by surface states or traps that affect the impedance measurements.[37] Redmond and Fitzmaurice found that Li^+ could change the E_{fb} from −1.8 V, without Li^+, to −0.6 V vs NHE with $Li^+ \geq 0.01$ M.[33] (2) It is difficult to accurately calibrate reference electrodes in nonaqueous solutions, especially when an aqueous reference (e.g., a calomel in MeCN)[32,33] is used: this forms a liquid junction potential that is difficult to reproduce.[38] (3) To the best of our knowledge, the measurements for TiO_2 were performed in solutions free of I^- or I_3^-. While the intercalation of Li^+ in TiO_2 seems to be predominant in setting the E_{fb} in MeCN,[33] I^- or I_3^- adsorption could have a large effect: Finklea tabulated data for E_{fb} in MeCN solutions that span over 2 V depending on electrolyte composition.[36] Thus, to avoid these problems we compare TiO_2 and Zn_2SnO_4 under the exact same conditions with nearly oxygen- and H_2O-free solutions and a nonaqueous reference.

Our results in Table 2 were obtained in solutions that closely resemble the electrolytes used in DSCs. For TiO_2 they agree with the usual values of V_{oc} of 0.7−0.8 V reported for

(31) Dung, D.; Ramsden, J.; Graetzel, M. *J. Am. Chem. Soc.* **1982**, *104*, 2977.
(32) Hagfeldt, A.; Graetzel, M. *Chem. Rev.* **1995**, *95*, 49.
(33) Redmond, G.; Fitzmaurice, D. *J. Phys. Chem.* **1993**, *97*, 1426.
(34) (a) O'Regan, B.; Graetzel, M.; Fitzmaurice, D. *J. Phys. Chem.* **1991**, *95*, 10525. (b) O'Regan, B.; Graetzel, M.; Fitzmaurice, D. *Chem. Phys. Lett.* **1991**, *183*, 89.
(35) Schumacher, R.; Teschner, D. M.; Heinzel, A. B. *Ber. Bunsen-ges. Phys. Chem.* **1982**, *86*, 1153.
(36) Finklea, H. O. Titanium dioxide (TiO2) and Stronium Titanate (SrTiO3). In *Semiconductor Electrodes*, 1st ed.; Finklea, H. O., Ed.; Elsevier: Amsterdam, 1988; Vol. 55; p 43.
(37) Frank, S. N.; Bard, A. J. *J. Am. Chem. Soc.* **1975**, *97*, 7427.
(38) Bard, A. J.; Faulkner, L. R. *Electrochemical Methods: Fundamentals and Applications*, 2nd ed.; John Wiley and Sons: New York, 2000; p 388.

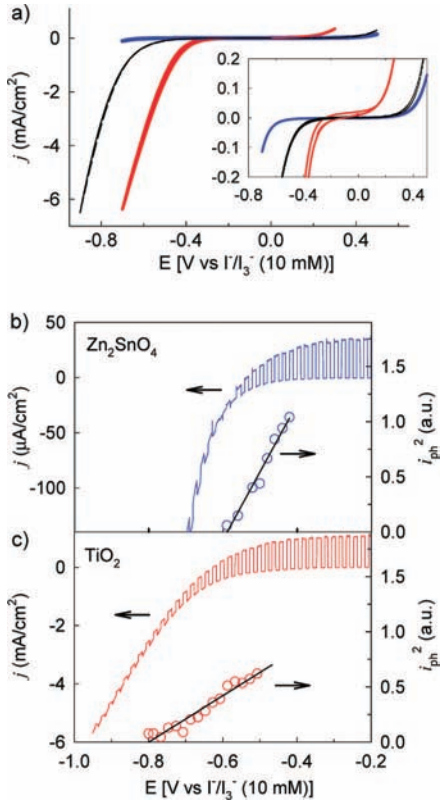

Figure 7. (a) Cyclic voltammetry of (black) bare FTO, (blue) Zn_2SnO_4/FTO, and (red) TiO_2/FTO in 0.7 M LiI, 0.05 M I_2 in MeCN, $\nu = 100$ mV/s; insert shows the detail at low current densities. (b and c) E_{fb} measurements of (a) Zn_2SnO_4 and (b) TiO_2 by the photocurrent (i_{ph}) onset method using the fit to Buttler theory for i_{ph}^2 (□). $\nu = 1$ mV/s, scan from negative side, 200 W Hg lamp, 0.05 Hz chopping frequency, in the same electrolyte as a.

I^-/I_3^- DSCs and with the trend that using *tert*-butyl pyridine (TBP) shifts the E_{fb} to more negative potentials by ca. 0.2 V, consistent with the observed increment in V_{oc} assigned to a shift in the E_{CB} to higher energies.[39] For Zn_2SnO_4 the E_{fb} depends strongly on electrolyte composition. Although Li^+ intercalation has been reported,[8] this does not seem to have the same predominant effect as on TiO_2 anatase. Our measurements explain the trend reported by our group[1] with the V_{oc} of $Zn_2SnO_4 < TiO_2$. However, Lana-Villarreal et al.[2] reported the opposite trend with the electrolyte of 0.7 M LiI, 0.05 M I_2 in 3-methoxypropionitrile.

Figure 7 shows the photoelectrochemical behavior of TiO_2 and Zn_2SnO_4 in 0.7 M LiI, 0.05 M I_2 in MeCN. Figure 7a shows the CVs obtained in the dark for these materials and for the FTO support. For TiO_2 the current becomes cathodic at $E < -0.4$ V vs I^-/I_3^- (10 mM) due to reduction of I_3^- on TiO_2 since FTO shows a much smaller current. The trend on the cathodic current is also in agreement with the previously reported data for the dark currents of cells made out of bare FTO and TiO_2/FTO reported by Gregg et al.[40] These authors point out that the dark currents of the CVs correlate quantitatively with the rates of recombination.

Zn_2SnO_4 has a much smaller cathodic current, indicating that the rate of I_3^- recombination is much smaller than that of TiO_2, as evident from the fact that the cathodic current decreases when the FTO surface is covered with Zn_2SnO_4, as expected for a passive layer. This is in sharp contrast to the higher currents obtained on anatase TiO_2/FTO surface. Interestingly, the anodic current assigned to I^- oxidation on TiO_2 is also higher than those of FTO and Zn_2SnO_4, and while the current of Zn_2SnO_4 is consistent with blocking the surface of FTO, the TiO_2 oxidation current is shifted negative for the I^- oxidation, indicating that the TiO_2 or some kind of TiO_2−FTO interaction and not the surface of the FTO exposed though defects on the TiO_2 are responsible for this electrochemical reaction.

Figure 7b and 7c shows the photoelectrochemical measurements of the E_{fb} using the i_{ph} onset method with −0.6 V for Zn_2SnO_4 and −0.8 V for TiO_2 vs I^-/I_3^- (10 mM). For TiO_2 while the i_{ph} is positive at $E > -0.8$ V, there is a net cathodic background superimposed with the anodic photocurrent. As the potential approaches −0.8 V the i_{ph} decreases and even changes signs at $E < -0.8$ V, consistent with the scan going through the E_{fb};[19] from the onset of i_{ph} we obtained $E_{fb} = -0.8$ V using the Buttler method to calculate E_{fb} with eq 5[18,19]

$$i_{ph}^2 \sim (E - E_{fb}) \tag{5}$$

The square of the i_{ph} vs E will have an x intercept of E_{fb}. These plots are shown in Figure 7b and 7c and show the trend of E_{fb} with Zn_2SnO_4 more positive than TiO_2. Combining these results with those in Figure 7a we can explain the trend of V_{oc} for $Zn_2SnO_4 > TiO_2$ observed in this electrolyte: although one would expect a large V_{oc} for TiO_2 from the E_{fb} of −0.8 V, this V_{oc} decreases more than 0.4 V by the larger recombination rate of e and I_3^-. For Zn_2SnO_4 this recombination is much smaller at potentials positive of the E_{fb} and explains the larger V_{oc} for Zn_2SnO_4 than TiO_2 reported[2] despite the higher energy of the TiO_2 CB.

Discussion

We studied the energetics of Zn_2SnO_4 NPs prepared by the hydrothermal method. NP films have been characterized by XRD and SEM, and the final material composition has been studied by ICP-MS.

The band-gap measurements are included in Table 1 along with previous experimental[3−6] and theoretical[7] reports for comparison. Our optical measurements show that Zn_2SnO_4 has a band gap of 3.6−3.7 eV with a direct-forbidden transition. Note that when fitting the experimental data to theory some reports have assumed allowed-direct transitions,[4,6] and this could account for some of the differences in E_g.

Our results best fit the theory of a direct-forbidden transition from the VB to a CB, which is in accordance with the more recent calculations of Segev and Wei of the Zn_2SnO_4 band structure.[7] The transition is direct because the conduction band minimum and valence band maximum are both located at the Γ point for both normal- and inverse-spinel Zn_2SnO_4. Due to the inversion symmetry the states at the

(39) (a) Boschloo, G.; Haggman, L.; Hagfeldt, A. *J. Phys. Chem. B* **2006**, *110*, 13144. (b) Nazeeruddin, M. K.; Kay, A.; Rodicio, I.; Humphry-Baker, R.; Mueller, E.; Liska, P.; Vlachopoulos, N.; Graetzel, M. *J. Am. Chem. Soc.* **1993**, *115*, 6382. (c) Schlichthorl, G.; Huang, S. Y.; Sprague, J.; Frank, A. J *J. Phys. Chem. B* **1997**, *101*, 8141. (d) Nakade, S.; Kanzaki, T.; Kubo, W.; Kitamura, T.; Wada, Y.; Yanagida, S. *J. Phys. Chem. B* **2005**, *109*, 3480. (e) Boschloo, G.; Lindström, H.; Magnusson, E.; Holmberg, A.; Hagfeldt, A. *J. Photochem. Photobiol., A* **2002**, *148*, 11.

(40) Gregg, B. A.; Pichot, F.; Ferrere, S.; Fields, C. L *J. Phys. Chem. B.* **2001**, *105*, 1422.

CB minimum and VB maximum have the same parity, which makes the transition forbidden.[7] For the inverse-spinel the calculations predict[7] that the VB maximum is derived mostly from O p and Sn 4d states with a minor contribution from Zn 3d states; in the CB minimum the O 2s and Zn 4s dominate over the Sn 5s contribution.

Our material has a Zn molar excess of ca. 3%. After heat treatment the lattice constant increases and the apparent optical E_g decreases to 3.2 eV. However, the E_g measured by photoelectrochemistry is still 3.86 ± 0.08 eV. The particle size calculated by XRD is within experimental error before and after heat treatment. At the average size of 25 nm and with the large particle dispersion of our NPs (see Figure 2) we do not expect any quantum confinement effect. Also, if the change in E_g was due to an increase in particle size after heat treatment one would expect the E_g measured after heat treatment with both optical and photoelectrochemical techniques to be smaller than the E_g before heat treatment.

In order to explain these results we propose that a minute excess of Zn^{2+}, possibly in the form of ZnO considering the solution of the hydrothermal reaction is basic, is carried with the Zn_2SnO_4 NPs after the hydrothermal reaction. After heat treatment the excess Zn^{2+} is incorporated into the Zn_2SnO_4, increasing the lattice constant and forming traps with an energy distribution tailing into the CB. Incorporation of Zn in the lattice has been further verified by XPS of the NPs films with the surface concentration of Zn decreasing after heat treatment.[41] Currently, we have not been able to determine whether the extra Zn functions as a donor or acceptor. We point out that the origin of the free carriers is still an open question for this material[4] since besides oxygen vacancies, excess Zn or Sn, and the corresponding possible changes in the spinel structure could be determinant in the free carrier concentration and mobility. For example, studies in amorphous and polycrystalline thin films have shown that Sn and Zn each have two distinct octahedral sites evident from Mössbauer spectroscopy.[21] This is due to local disorder in the Zn and Sn sites, although is not clear if this is the result of differences in the stoichiometry or defects in the crystal structure,[21,42] while this disorder could cause the lower mobility of Zn_2SnO_4 with respect to Cd_2SnO_4.[21]

The traps in the Zn_2SnO_4 matrix modify its optical absorption properties, inducing an apparent decrease of E_g. However, we believe these traps are localized and do not participate in the photoelectrochemical processes. Thus, the E_g of 3.86 ± 0.08 eV measured by photoelectrochemistry is expected to be the fundamental VB to CB transitions. Due to the 20 nm resolution of the photoelectrochemical measurement we propose the E_g = 3.6−3.7 eV from optical transmittance.

Flat band potentials of Zn_2SnO_4 have been measured by the photoelectrochemical onset method. The E_{fb} changes with pH with a 59 mV/pH slope. This slope has been reported previously for TiO_2 and other oxides and indicates that in aqueous solutions the surface of the Zn_2SnO_4 is in equilibrium with H^+ and OH^- specifically adsorbed and the relative charges of H^+ and OH^- set the potential across the Helmholtz layer.[25] Overall, the E_{fb} of Zn_2SnO_4 is positive with respect to TiO_2 anatase by ca. 0.1 V in the electrochemical scale (0.1 eV more negative in the solid-state scale vs vacuum) despite the larger E_g of Zn_2SnO_4 (3.6−3.7 eV) than of anatase (3.2 eV).

The measurements in MeCN are relevant to DSCs since they contain the same electrolytes used for the devices. Interestingly, the traps in Zn_2SnO_4 are not apparent, and thus, they do not seem to be catalytic toward I^- or I_3^-; also, the increase of photocurrent slope observed in aqueous solution is not present either, consistent with the expectation that the material would be more stable in nonaqueous solvents. Our results explain the observed experimental results in DSCs with the E_{fb} of Zn_2SnO_4 more positive than that of TiO_2, causing a smaller V_{oc} for Zn_2SnO_4 in a previous report from our group.[1] The report of Lana-Villareal et al.[2] of a smaller V_{oc} for TiO_2 is due to the larger rates of recombination in their electrolyte. Zn_2SnO_4 shows overall a smaller rate of e and I_3^- recombination near the E_{cb} than that of TiO_2. The lower recombination rate for Zn_2SnO_4 also supports the finding that the e lifetime in Zn_2SnO_4 is larger than that in TiO_2.[2] We found that this rate of recombination is significant for TiO_2 at potentials positive of the E_{cb}, indicating that this is caused by states that lie at lower energy than the CB but are somewhat catalytic toward reduction of I_3^-. The nature of these states is the subject of current investigation in our group and is interesting since they seem to be responsible for oxidation of I^- normally thought to occur on the FTO substrate.

The results in Table 2 also show that it should be possible to tune the E_{fb} of Zn_2SnO_4 by controlling the electrolyte composition/semiconductor interface. Note that the DSCE increases the energy of E_{CB} for Zn_2SnO_4 while it decreases it for TiO_2, so the electrolyte/semiconductor interactions may be very specific to the material. This opens the possibility of increasing V_{oc} using interfacial interactions to shift the E_{CB} to higher energies. From the CV the Zn_2SnO_4 has a much lower recombination rate near the E_{CB}. This will avoid the problem normally associated with TiO_2 of lower η at higher V_{OC} due to e and I_3^- recombination losses at traps below the CB.[43]

Conclusions

The band structure of Zn_2SnO_4 prepared by the hydrothermal method has been studied by photoelectrochemistry and optical methods. The optical and electronic properties of the material have been correlated with our characterization of the material in terms of structure (XRD and SEM) and composition (ICP-MS).

On the basis of our results, we believe the large variability in the E_g reports for Zn_2SnO_4 to be due to differences in the stoichiometry (see Table 1) and propose a fundamental E_g of 3.6−3.7 eV.

This also confirms that Zn_2SnO_4 is an interesting material for photoanode supports for dye-sensitized solar cells since the large band-to-band transition substantially diminishes photobleaching and presents a lower electron−triiodide recombination rate. On the other hand, Zn_2SnO_4 would not be an interesting material for water splitting compared to TiO_2 due to the lower energy of the CB and the higher E_g unless doping procedures can tune the E_{fb} and E_g to allow H^+ photoreduction with lower excitation energy than TiO_2.

(41) Alpuche-Aviles, M.; Wu, Y. Unpublished Results, 2009.

(42) Nikolic, M. V.; Satoh, K.; Ivetic, T.; Paraskevopoulos, K. M.; Zorba, T. T.; Blagojevic, V.; Mancic, L.; Nikohic, P. M. *Thin Solid Films* **2008**, *516*, 6293.

(43) (a) Nazeeruddin, M. K.; Humphry-Baker, R.; Liska, P.; Gratzel, M. *J. Phys. Chem. B.* **2003**, *107*, 8981. (b) Zhu, K.; Kopidakis, N.; Neale, N. R.; vandeLagemaat, J.; Frank, A. J. *J. Phys. Chem. B* **2006**, *110*, 25174. (c) Wang, Q.; Ito, S.; Gratzel, M.; Fabregat-Santiago, F.; Mora-Sero, I.; Bisquert, J.; Bessho, T.; Imai, H. *J. Phys. Chem. B* **2006**, *110*, 25210. (d) Bisquert, J.; Vikhrenko, V. S. *J. Phys. Chem. B* **2004**, *108*, 2313 .

We note that we are neglecting the difference between E_{cb}, and E_{fb}; this difference is a strong function of the doping density, and here we only present our initial results. Future work will include studying how excess Zn or Sn affects the doping density and degree of inversion of the spinel structure and, in turn, the *e*-transport properties. Understanding the relationship between structure, transport properties, and E_{fb} of Zn_2SnO_4 could allow tuning this material to improve the efficiency of dye-sensitized solar cells.

Acknowledgment. Y.W. acknowledges support from the U.S. Department of Energy under Award No. DE-FG02-07ER46427 and a Research Corporation Cottrell Scholar Award. Y.W. also thanks Professor Patrick Woodward and Matthew J. O'Malley for informative discussions.

JA806719X